A&A 451, 759–766 (2006)
DOI: 10.1051/0004-6361:20054454

Astronomy & Astrophysics

COSMOGRAIL: the COSmological MOnitoring of GRAvItational Lenses

III. Redshift of the lensing galaxy in eight gravitationally lensed quasars⋆

A. Eigenbrod[1], F. Courbin[1], G. Meylan[1], C. Vuissoz[1], and P. Magain[2]

[1] Laboratoire d'Astrophysique, École Polytechnique Fédérale de Lausanne (EPFL), Observatoire, 1290 Sauverny, Switzerland
[2] Institut d'Astrophysique et de Géophysique, Université de Liège, Allée du 6 août 17, Sart-Tilman, Bat. B5C, 4000 Liège, Belgium

Received 1 November 2005 / Accepted 21 December 2005

ABSTRACT

Aims. We measure the redshift of the lensing galaxy in eight gravitationally lensed quasars in view of determining the Hubble parameter H_0 from the time delay method.
Methods. Deep VLT/FORS1 spectra of lensed quasars are spatially deconvolved in order to separate the spectrum of the lensing galaxies from the glare of the much brighter quasar images. A new observing strategy is devised. It involves observations in Multi-Object-Spectroscopy (MOS) which allows the simultaneous observation of the target and of several PSF and flux calibration stars. The advantage of this method over traditional long-slit observations is a much more reliable extraction and flux calibration of the spectra.
Results. For the first time we measure the redshift of the lensing galaxy in three multiply-imaged quasars: SDSS J1138+0314 ($z_{\rm lens} = 0.445$), SDSS J1226−0006 ($z_{\rm lens} = 0.517$), SDSS J1335+0118 ($z_{\rm lens} = 0.440$), and we give a tentative estimate of the redshift of the lensing galaxy in Q 1355−2257 ($z_{\rm lens} = 0.701$). We confirm four previously measured redshifts: HE 0047−1756 ($z_{\rm lens} = 0.407$), HE 0230−2130 ($z_{\rm lens} = 0.523$), HE 0435−1223 ($z_{\rm lens} = 0.454$) and WFI J2033−4723 ($z_{\rm lens} = 0.661$). In addition, we determine the redshift of the second lensing galaxy in HE 0230−2130 ($z_{\rm lens} = 0.526$). The spectra of all lens galaxies are typical for early-type galaxies, except for the second lensing galaxy in HE 0230−2130 which displays prominent [OII] emission.

Key words. gravitational lensing – cosmological parameters – quasars: general

1. Introduction

Gravitationally lensed quasars have become a truly efficient source of new astrophysical applications, since the discovery of the first case by Walsh et al. (1979). These objects are potentially useful for measuring the Hubble parameter H_0 from the time delay between their lensed images (Refsdal 1964), assuming a model for the mass distribution in the lensing galaxy. Conversely, for an assumed or measured value of H_0, the mass distribution in the lens can be reconstructed from the time delay measurement. The study of lensed quasars is therefore a "no-lose" game, either because of its cosmological implications (H_0) or for the study of galaxy formation and evolution through the determination of detailed mass maps for lensing galaxies, especially their dark matter content.

The second most important application of quasar lensing involves microlensing by stars in the lensing galaxy. Microlenses produce chromatic magnification events in the light curve of the images of the source, as they cross their line of sight. The amplitude, duration and frequency of the events depend on the transverse velocity of stars in the lensing galaxy, on their surface density, and on the relative sizes of the microlensing caustics with respect to the regions of the source affected by microlensing. Photometric monitoring of lensed quasars in several bands or, better, spectrophotometric monitoring can therefore yield constraints on the energy profile of quasar accretion disks and on the size of the various emission line regions (e.g. Agol & Krolik 1999; Mineshige & Yonehara 1999; Abajas et al. 2002).

All the above applications of quasar lensing require the knowledge of the redshift of the lensing galaxy, which is frequently hidden in the glare of the quasar images. The present paper is part of a larger effort to carry out long term photometric monitoring of lensed quasars in the context of COSMOGRAIL (e.g. Eigenbrod et al. 2005). In this paper we focus on the determination of the redshifts of the lensing galaxies in several gravitationally lensed quasars, using deep spectra obtained with the ESO Very Large Telescope (VLT). The targets were simply selected in function of their visibility during the period of observation.

2. VLT spectroscopy

2.1. Observations

We present observations for eight gravitationally lensed quasars, in order to determine the redshift of the lensing galaxy. The targets are HE 0047−1756, HE 0230−2130, HE 0435−1223, SDSS J1138+0314, SDSS J1335+0118, Q 1355−2257 (also known as CTQ 327), SDSS J1226−0006 and WFI J2033−4723.

Our spectroscopic observations are acquired with the FOcal Reducer and low dispersion Spectrograph (FORS1), mounted

⋆ Based on observations made with the ESO-VLT Unit Telescope 2 Kueyen (Cerro Paranal, Chile; Programs 074.A-0563 and 075.A-0377, PI: G. Meylan). and on archive data taken with the ESO-VLT Unit Telescope 1 Antu (Cerro Paranal, Chile; Program 064.O-0259(A), PI: L. Wisotzki).

Table 1. Journal of the observations of HE 0047−1756. Grism and filter: G300V+GG435. HR collimator: 0.1″ per pixel. Slitlets width: 1.0″ (R = 210 at 5900 Å).

ID	Date	Seeing [″]	Airmass	Weather
1	18/07/2005	0.49	1.281	Photometric
2	18/07/2005	0.53	1.191	Photometric

Table 2. Journal of the observations of HE 0230−2130. Grism and filter: G600R+GG435. SR collimator: 0.2″ per pixel. Slitlets width: 0.5″ (R = 1910 at 6200 Å).

ID	Date	Seeing [″]	Airmass	Weather
1	15/12/2004	0.60	1.166	Light clouds
2	15/12/2004	0.58	1.248	Light clouds
3	01/03/2005	0.78	1.800	Photometric

on the ESO Very Large Telescope. Very importantly, all the observations are carried out in the MOS mode (Multi Object Spectroscopy). This strategy allows the simultaneous observation of the main target and of several stars used both as flux calibrators and as reference PSF to spatially deconvolve the data.

Most of our targets are observed with the high-resolution collimator, allowing us to observe simultaneously eight objects over a field of view of $3.4' \times 3.4'$ with a pixel scale of 0.1″. However, because few suitable PSF stars are visible in the vicinity of SDSS J1226−0006 and HE 0230−2130, the observations for these two objects use the standard-resolution collimator, which has a field of view of $6.8' \times 6.8'$ and a pixel size of 0.2″.

We use the GG435 order sorting filter in combination with the G300V grism for all objects, except HE 0230−2130 for which we use the G600R grism. The G300V grism gives a useful wavelength range $4450 < \lambda < 8650$ Å and a scale of 2.69 Å per pixel in the spectral direction. This setup has a spectral resolution $R = \lambda/\Delta\lambda \simeq 200$ at the central wavelength $\lambda = 5900$ Å for a 1.0″ slit width in the case of the high resolution collimator. The choice of this grism favors spectral coverage rather than spectral resolution as the observations are aimed at measuring unknown lens redshifts. The combination of the G600R grism with the GG435 filter used for HE 0230−2130 has a wavelength range of $5250 < \lambda < 7450$ Å with a pixel scale of 1.08 Å in the spectral direction. This gives a higher spectral resolution of $R \simeq 1200$ at the central wavelength $\lambda = 6270$ Å for a slit width of 1.0″ and with the standard resolution collimator.

We choose slitlets of various widths, depending on the brightness of the target and on the configuration of the quasar images. The slit width is chosen so that it matches the seeing requested for the service-mode observations and minimizes lateral contamination by the quasar images. Our observing sequences consist of a short acquisition image, an "image-through-slit" check, followed by one or two consecutive deep spectroscopic exposures. All individual exposures for all objects are 1400 s long. The journals of the observations are given in Tables 1 to 8. The through-slit images are displayed in Figs. 1 to 8, where the epochs refer to the exposure numbers in Tables 1 to 8.

For every object we center at least three slitlets on foreground stars and one slitlet on the lensing galaxy. The mask is rotated to a Position Angle that avoids clipping of any quasar image. This is mandatory to carry out spatial deconvolution of the spectra. The spectra of the PSF stars are also used to cross-calibrate the flux scale as the data are taken at different airmasses and at different dates. Three spectrophotometric standard stars are used to carry out the relative flux calibration, i.e. EG 21, LTT 3218, and LTT 6248.

Table 3. Journal of the observations for HE 0435−1223. Grism and filter: G300V+GG435. HR collimator: 0.1″ per pixel. Slitlets width: 1.0″ (R = 210 at 5900 Å).

ID	Date	Seeing [″]	Airmass	Weather
1	11/10/2004	0.47	1.024	Photometric
2	11/10/2004	0.45	1.028	Photometric
3	12/10/2004	0.46	1.024	Photometric
4	12/10/2004	0.53	1.028	Photometric
5	11/11/2004	0.57	1.093	Photometric
6	11/11/2004	0.56	1.145	Photometric

Table 4. Journal of the observations for SDSS J1138+0314. Grism and filter: G300V+GG435. HR collimator: 0.1″ per pixel. Slitlets width: 1.0″ (R = 210 at 5900 Å).

ID	Date	Seeing [″]	Airmass	Weather
1	10/05/2005	0.82	1.191	Photometric
2	11/05/2005	0.70	1.155	Photometric
3	11/05/2005	0.67	1.133	Photometric
4	11/05/2005	0.66	1.132	Photometric
5	11/05/2005	0.64	1.148	Photometric

Table 5. Journal of the observations for SDSS J1226−0006. Grism and filter: G300V+GG435. SR collimator: 0.2″ per pixel. Slitlets width: 1.0″ (R = 400 at 5900 Å).

ID	Date	Seeing [″]	Airmass	Weather
1	16/05/2005	0.85	1.109	Photometric
2	16/05/2005	0.84	1.099	Photometric
3	16/05/2005	0.92	1.105	Photometric
4	16/05/2005	1.02	1.125	Photometric
5	16/05/2005	0.78	1.221	Photometric
6	16/05/2005	0.89	1.299	Photometric
7	16/05/2005	0.82	1.422	Photometric
8	16/05/2005	0.88	1.576	Photometric

Table 6. Journal of the observations for SDSS J1335+0118. Grism and filter: G300V+GG435. HR collimator: 0.1″ per pixel. Slitlets width: 1.0″ (R = 210 at 5900 Å).

ID	Date	Seeing [″]	Airmass	Weather
1	03/02/2005	0.73	1.167	Photometric
2	03/02/2005	0.71	1.133	Photometric
3	03/03/2005	0.69	1.112	Photometric
4	03/03/2005	0.77	1.123	Photometric
5	03/03/2005	0.68	1.153	Photometric
6	03/03/2005	0.62	1.198	Photometric

Table 7. Journal of the observations for Q 1355−2257. Grism and filter: G300V+GG435. HR collimator: 0.1″ per pixel. Slitlets width: 1.0″ (R = 210 at 5900 Å).

ID	Date	Seeing [″]	Airmass	Weather
1	05/03/2005	0.68	1.016	Photometric
2	05/03/2005	0.73	1.040	Photometric
3	20/03/2005	0.63	1.038	Photometric
4	20/03/2005	0.54	1.015	Photometric
5	20/03/2005	0.57	1.105	Photometric
6	20/03/2005	0.56	1.166	Photometric

Table 8. Journal of observations for WFI J2033−4723. Grism and filter: G300V+GG435. HR collimator: 0.1″ per pixel. Slitlets width: 1.4″ (R = 160 at 5900 Å).

ID	Date	Seeing [″]	Airmass	Weather
1	13/05/2005	0.50	1.256	Light clouds
2	13/05/2005	0.58	1.198	Light clouds
3	13/05/2005	0.60	1.148	Light clouds
4	13/05/2005	0.48	1.117	Light clouds
5	13/05/2005	0.53	1.095	Light clouds

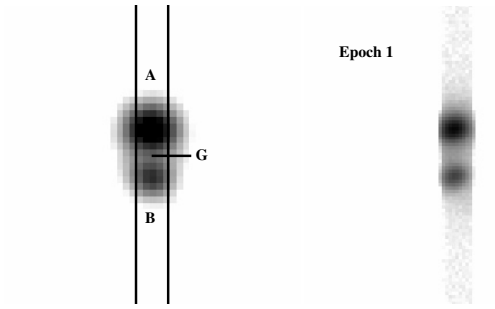

Fig. 1. HE 0047−1756. Slit width: 1.0″. Mask PA: 10°.

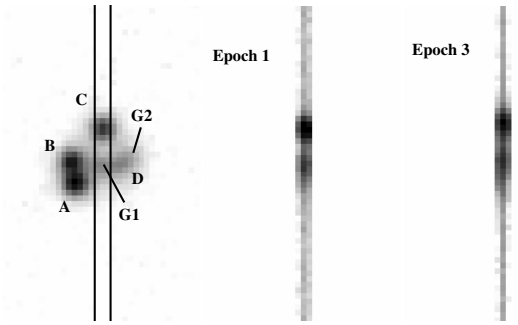

Fig. 2. HE 0230−2130. Slit width: 0.5″. Mask PA: −60°.

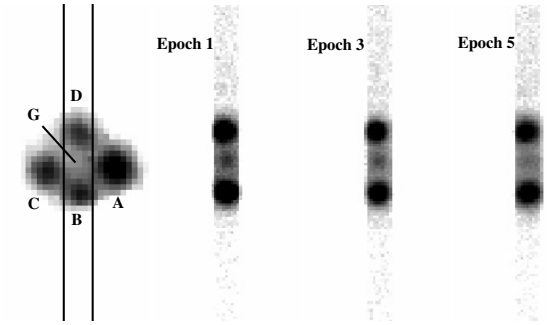

Fig. 3. HE 0435−1223. Slit width: 1.0″. Mask PA: −164°.

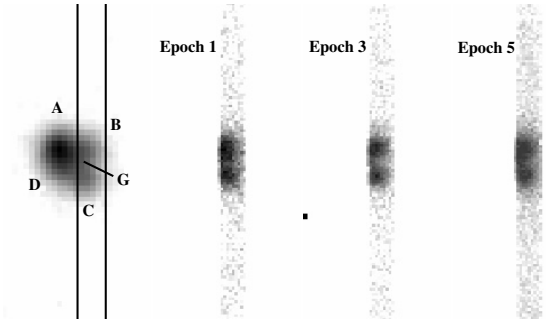

Fig. 4. SDSS J1138+0314. Slit width: 1.0″. Mask PA: −84°.

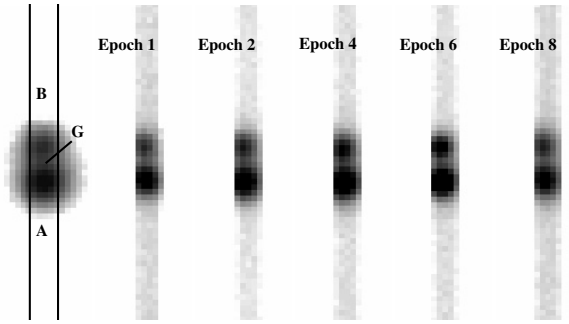

Fig. 5. SDSS J1226−0006. Slit width: 1.0″. Mask PA: −90°.

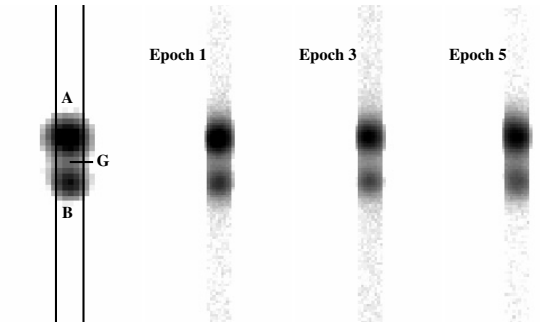

Fig. 6. SDSS J1335+0118. Slit width: 1.0″. Mask PA: 43°.

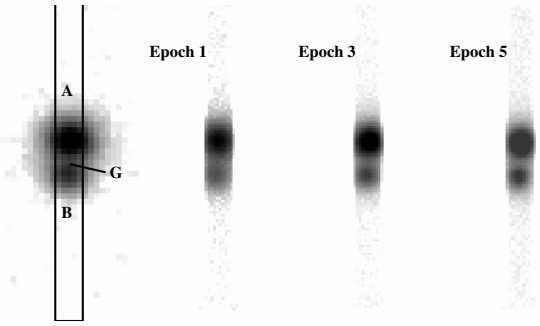

Fig. 7. Q 1355−2257. Slit width: 1.0″. Mask PA: −78°.

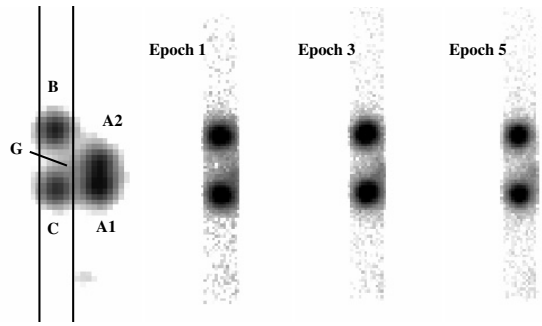

Fig. 8. WFI J2033−4723. Slit width: 1.4″. Mask PA: −82°.

In addition to our own data, we retrieve VLT/FORS1 data from the archive for HE 0230−2130. These data were acquired on 18 October 1999 for program 064.O-0259(A). They used the long slit mode with the standard resolution collimator (0.2″ per pixel), the G600R grism, and the order sorting filter GG435. The useful wavelength range is the same as for the MOS observations, i.e., 5250 $< \lambda <$ 7450 Å with a pixel scale of 1.08 Å in the spectral direction.

2.2. Reduction and deconvolution

We carry out the standard bias subtraction and flat field correction of the spectra using IRAF[1]. The flat field is created for each slitlet from five dome exposures using cosmic ray rejection. It is then normalized by averaging 45 lines along the spatial direction, rejecting the 20 highest and 20 lowest pixels. The result is then block replicated to match the physical size of the individual flat fields.

Wavelength calibration is obtained from numerous emission lines in the spectrum of helium-argon lamps. The wavelength solution is fitted in two dimensions to each slitlet of the MOS mask. The fit uses a fifth order Chebyshev polynomial along the spectral direction and a fourth order Chebyshev polynomial fit along the spatial direction. Each spectrum is interpolated following this fit using a cubic interpolation. This procedure ensures that the sky lines are well aligned with the columns of the CCD after wavelength calibration.

The sky background is then removed by fitting and subtracting a second order Chebyshev polynomial in the spatial direction to the areas of the spectrum that are not illuminated by the object.

Finally, we remove the cosmic rays as follows. First we shift the spectra in order to align them spatially (this shift is only a few tenths of a pixel). Second, we create a combined spectrum for each object from all exposures, removing the lower and higher pixels, after applying appropriate flux scaling. The combined spectrum obtained in that way is cosmic ray cleaned and is used as a reference template to clean the individual spectra. For each MOS mask the object slitlet and the PSF slitlets are reduced exactly in the same way.

A flux cross-calibration of the spectra taken at different airmasses or dates is needed before combining them into one final spectrum. This is done efficiently using the spectra of the PSF stars as references, as described in Eigenbrod et al. (2006). The reference stars are assumed to be non-variable and a ratio spectrum is created for each star, i.e. we divide the spectrum of the star by the spectrum of the same star in the other exposures. This is done for at least two stars in each mask and we check that the response curves derived using different stars are compatible. The dispersion between the response curves obtained in that way is about 2%. A mean correction curve is then computed and applied to each two-dimensional spectrum. The individual spectra for each object are finally combined.

The archive data of HE 0230−2130 consist of one single long slit spectrum. The bias subtraction, flatfielding, wavelength calibration and background removal are done in exactly the same way as for the MOS spectra. The cosmic ray removal is done using the IRAF packages for single-image data. The flux calibration is done using three standard stars: G93−48, LTT 7987, LTT 9239, taken on the same night as the science frame.

2.3. Deconvolution and extraction of the MOS spectra

Even though the seeing values are good for most spectra, the lensing galaxy is often close enough to the brighter quasar images to be affected by significant contamination from the wings of the PSF. For this reason, the spectral version of the MCS deconvolution algorithm (Magain et al. 1998; Courbin et al. 2000) is used in order to separate the spectrum of the lensing galaxy from the spectra of the quasar images. The MCS algorithm uses the spatial information contained in the spectrum of a reference PSF, which is obtained from the slitlets positioned on the isolated stars. The final normalized PSF is a combination of at least three different PSF spectra. The deconvolved spectra are not only sharpened in the spatial direction, but also decomposed into a "point-source channel" containing the spectra of the quasar images, and a "extended channel" containing the spectra of everything in the image which is not a point-source, i.e. in this case the spectrum of the lensing galaxy.

The deconvolved spectra of the lensing galaxies are extracted and smoothed with a 10 Å box. Figures 9 to 16 display the final one-dimensional spectra, where the Ca II H & K absorption lines are obvious, as well as the 4000 Å Balmer break, and the G-band typical for CH absorption. In some cases, we identify a few more features that are labeled in the individual figures. The identified lines are used to determine the redshift of the lensing galaxies given in Table 9. We compute the 1-σ error as the standard deviation between all the measurements of the individual lines. The absence of emission lines in all spectra indicates that the observed lensing galaxies are gas-poor early-type galaxies.

In most cases, no trace of the quasar broad emission lines is seen in the spectrum of the lensing galaxy, indicative of an accurate decomposition of the data into the extended (lens) and point source (quasar images) channels. Only our VLT spectrum of the lensing galaxy of HE 0230−2130 is suffering from residuals of the quasar broad emission lines, probably due to lateral contamination by images A and B of the quasar. This additional source of contamination is circumvented by subtracting a scaled version of the spectrum of quasar image C to the spectrum of the lensing galaxy. The flux calibration of this particular lens might therefore be less accurate than for the other objects. Note, however, that this procedure was only applied to HE 0230−2130.

3. Notes on individual objects

HE 0047−1756: a doubly imaged quasar discovered by Wisotzki et al. (2004). It has a redshift of $z = 1.67$ and a maximum image separation of 1.44″. The redshift of the lensing galaxy has recently been measured by Ofek et al. (2005) at $z_{\rm lens} = 0.408$. We confirm this result, with $z_{\rm lens} = 0.407 \pm 0.001$, and present a much higher signal-to-noise spectrum in Fig. 9. An elliptical galaxy template matches well the spectrum of the lens.

HE 0230−2130: this quadruply imaged $z = 2.162$ quasar was discovered by Wisotzki et al. (1999). It has a maximum image separation of 2.15″ and two lensing galaxies. The main lensing galaxy, G1, is located between the four quasar images. A second, fainter lens is located outside the area defined by the quasar images, close to the faint quasar image D (Fig. 17). The spectrum of G1 is shown in Fig. 10. Our redshift ($z_{\rm lens} = 0.523 \pm 0.001$) is in very good agreement with the result $z_{\rm lens} = 0.522$ of Ofek et al. (2005). The spectrum matches well that of an early-type galaxy. The spectrum of the second lensing galaxy G2 is extracted from the archive long-slit spectrum presented in Sect. 4.

HE 0435−1223: this quadruply imaged quasar, discovered by Wisotzki et al. (2002), has a redshift of $z = 1.689$ and has a maximum image separation of 2.56″, hence with little contamination of the lens spectrum by the quasar images. The redshift of the lensing galaxy has already been measured (Morgan et al. 2005; Ofek et al. 2005) at $z_{\rm lens} = 0.455$. We confirm this result, with $z_{\rm lens} = 0.454 \pm 0.001$, and present a much higher signal-to-noise spectrum in Fig. 11. A S0 galaxy template matches well the spectrum of the lens.

[1] IRAF is distributed by the National Optical Astronomy Observatories, which are operated by the Association of Universities for Research in Astronomy, Inc., under cooperative agreement with the National Science Foundation.

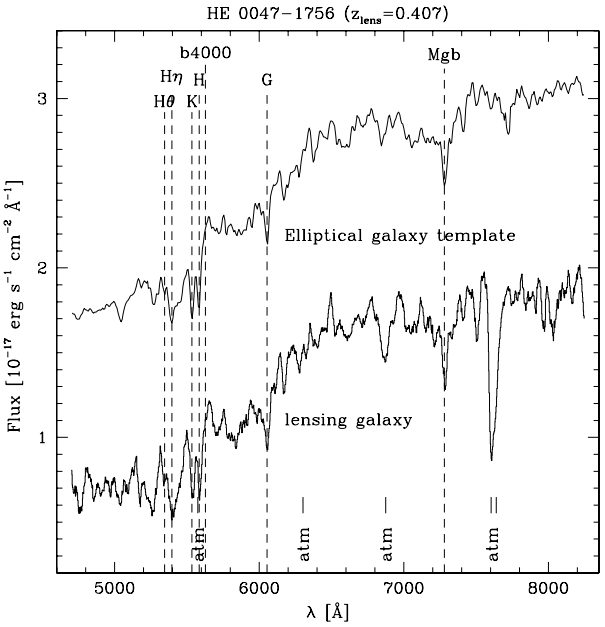

Fig. 9. Spectrum of the lens in HE 0047−1756. The total integration time is 2800 s. The template spectrum of a redshifted elliptical galaxy is shown for comparison (Kinney et al. 1996).

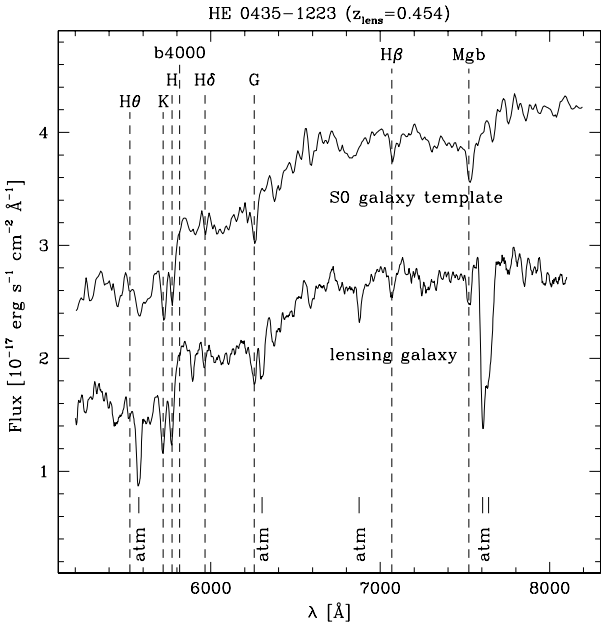

Fig. 11. Spectrum of the lens in HE 0435−1223. The total integration time is 8400 s. The template spectrum of a redshifted S0 galaxy is shown (Kinney et al. 1996).

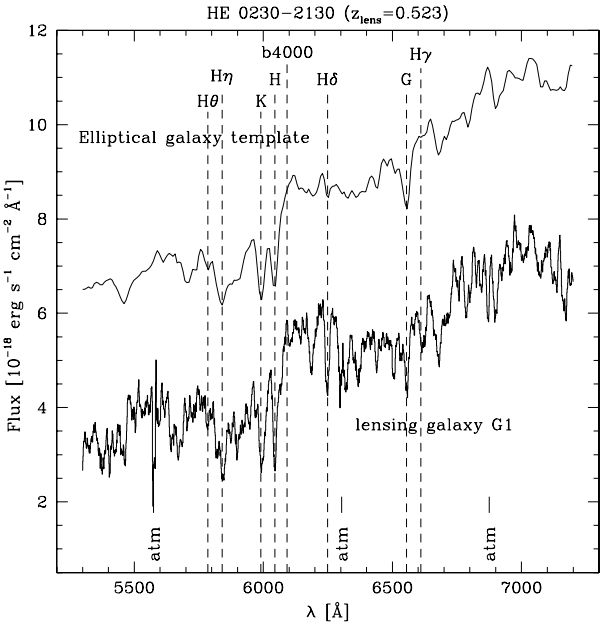

Fig. 10. Spectrum of the lensing galaxy G1 in HE 0230−2130, as obtained by combining the data for the three epochs, i.e. a total integration time of 4200 s. A scaled version of the spectrum of quasar image C is subtracted to the spectrum of the lensing galaxy, in order to remove lateral contamination by the quasar images A and B (see text).

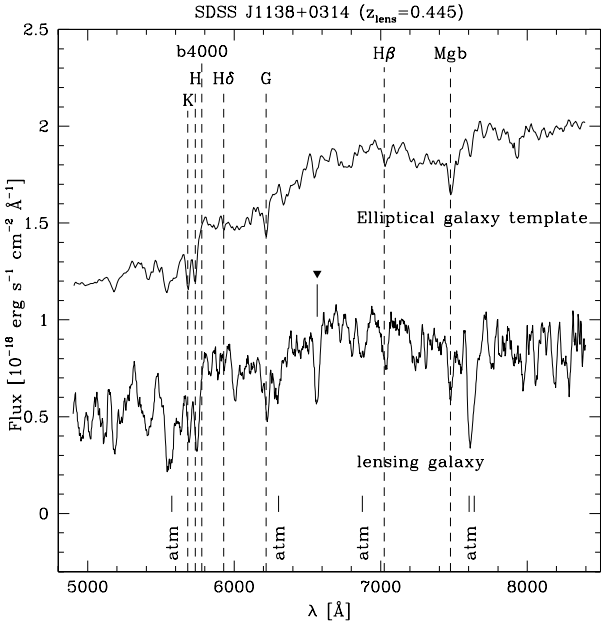

Fig. 12. Spectrum of the lens in SDSS J1138+0314. The total integration time is 7000 s. The absorption feature marked by the black triangle is probably residual light of the quasar images. The C III] emission of the quasar falls exactly at this wavelength.

SDSS J1138+0314: this quadruply imaged quasar was discovered in the course of the Sloan Digital Sky Survey (SDSS) by Burles et al. (2005). This lensed quasar has a maximum image separation of 1.46″. We obtain high signal-to-noise spectra of the quasar and determine its redshift $z = 2.438$. There is very little doubt that this system is lensed. The lensing galaxy is seen on archival HST/NICMOS images. We measure $z_{\rm lens} = 0.445 \pm 0.001$ (Fig. 12).

SDSS J1226−0006: a doubly imaged quasar at $z = 1.120$ found in the course of the Sloan Digital Sky Survey (SDSS) by Inada et al. (2005). This system is doubtlessly lensed, as the lensing galaxy is seen on archival HST/ACS images, between both quasar images, at only 0.4″ away from image A. We measure $z_{\rm lens} = 0.516 \pm 0.001$ (Fig. 13). The spectrum of the lensing galaxy is well matched by the spectrum of an elliptical galaxy.

SDSS J1335+0118: a doubly imaged quasar with a 1.56″ separation, discovered by Oguri et al. (2004). The quasar is at

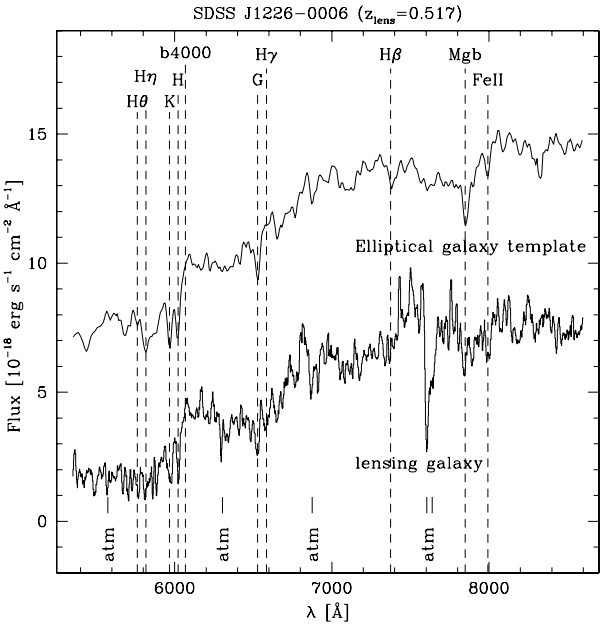

Fig. 13. Spectrum of the lens in SDSS J1226−0006. The total integration time is 11 200 s.

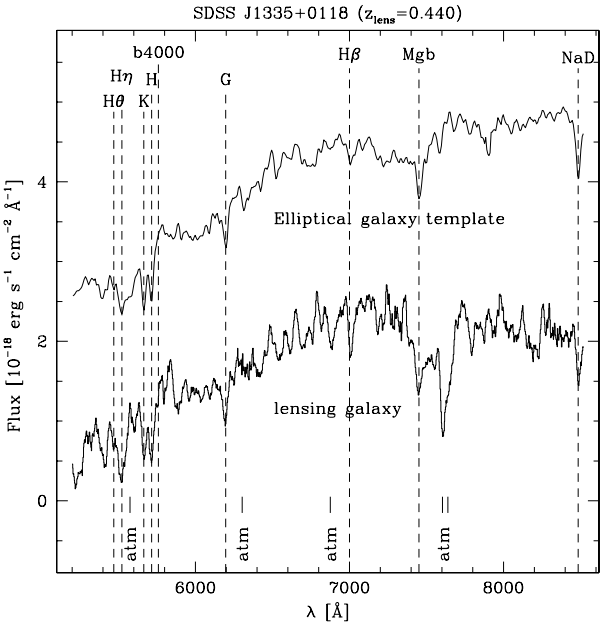

Fig. 14. Spectrum of the lens in SDSS J1335+0118. The total integration time is 8400 s.

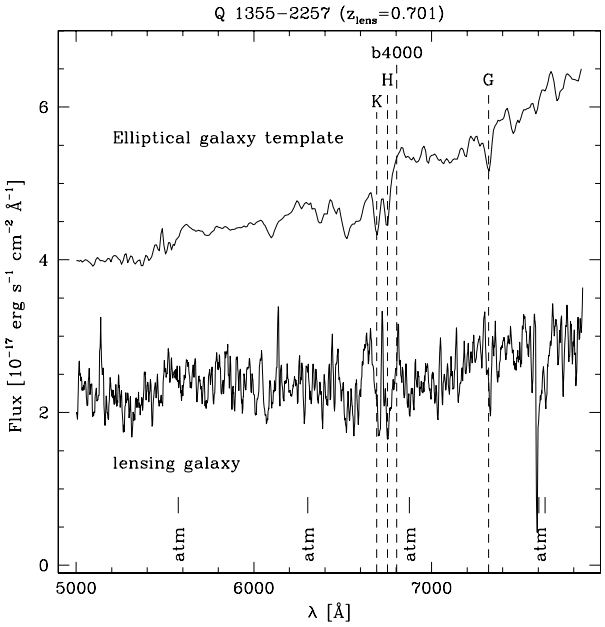

Fig. 15. Spectrum of the lens in Q 1355−2257. The total integration time is 8400 s. Given the low signal-to-noise of this spectrum we can not securely determine the lens redshift.

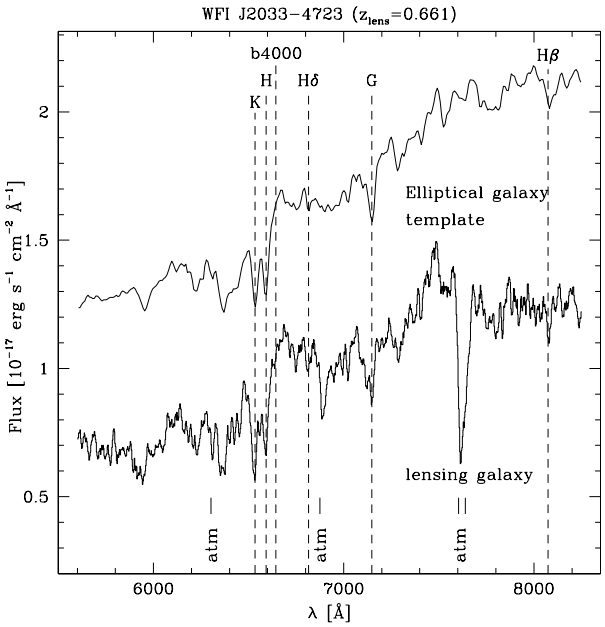

Fig. 16. Spectrum of the lens in WFI J2033−4723. The total integration time is 7000 s.

$z = 1.57$ and the spectra of the quasar images show evidence of strong absorption systems at lower redshifts. Based on the color of the galaxy, Oguri et al. (2004) conclude that the lens galaxy is consistent with an early-type galaxy at $z \lesssim 0.5$. Our spectrum (Fig. 14) is indeed that of an early-type galaxy. Its redshift $z_{\rm lens} = 0.440 \pm 0.001$ has not been measured before.

Q 1355−2257 (CTQ 327): this doubly imaged quasar has a redshift of $z = 1.373$ and was discovered by Morgan et al. (2003). The quasar images are separated by 1.23″ and the redshift of the lensing galaxies has been estimated by Morgan et al. (2003) to lie in the redshift range $0.4 < z_{\rm lens} < 0.6$. The extraction of the spectrum of the lensing galaxy is particularly difficult because the galaxy lies at only 0.29″ away from quasar image B and because it is 7 mag fainter. We show the deconvolved spectrum of the lensing galaxy in Fig. 15. Given the low signal-to-noise of this spectrum we cannot securely determine the lens redshift; we can only give a tentative estimate of $z_{\rm lens} = 0.701$.

WFI J2033−4723: Morgan et al. (2004) discovered this quadruply lensed quasar with maximum image separation of 2.53″ and redshift $z = 1.66$. Ofek et al. (2005) recently measured the lens redshift $z_{\rm lens} = 0.658$. The lensing galaxy spectrum shown in Fig. 16 is matched by an elliptical or S0 galaxy template with a redshift of $z_{\rm lens} = 0.661 \pm 0.001$. Our measured

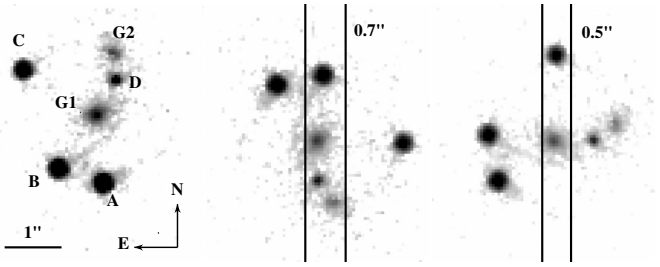

Fig. 17. *Right*: HST image of HE 0230−2130 taken with the WFPC2 instrument in the F814W filter. The pixel scale is 0.05″. *Middle*: same image but with a position angle of −160°. We show in overlay a 0.7″ slit which corresponds to the observational setup used to take the long-slit spectrum (program 064.O-0259(A) archive data). *Left*: for comparison, we show the slit used for our MOS observations. The position angle is −60° and the slit has a width of 0.5″. Negative angles are counted clockwise from North.

Table 9. Redshift values determined for the lensing galaxies in the eight gravitational lenses. Only a tentative redshift is given for Q 1355−2257. See Section 4 for more details about the second lens G2 in HE 0230−2130.

Object	z_{lens}
HE 0047−1756	0.407 ± 0.001
HE 0230−2130, G1	0.523 ± 0.001
HE 0230−2130, G2	0.526 ± 0.002
HE 0435−1223	0.454 ± 0.001
SDSS J1138+0314	0.445 ± 0.001
SDSS J1226−0006	0.517 ± 0.001
SDSS J1335+0118	0.440 ± 0.001
Q 1355−2257	0.701(?)
WFI J2033−4723	0.661 ± 0.001

redshift is compatible with but slighly higher than the one reported by Ofek et al. (2005).

4. The second lens in HE 0230−2130

The long-slit archive FORS1 spectrum of HE 0230−2130 is taken with the slit centered on the quasar images B and D (middle panel in Fig. 17). The two-dimensional sky-subtracted spectrum is shown in Fig. 18, where a hint of an emission line can already be seen at the spatial location of lens G2 along the slit.

As no PSF star is available the data have to be deconvolved in a different way than the MOS spectra. We proceed in an iterative way. First, we cut the spectrum in two along the spectral direction and determine a first estimate of the reference PSF spectrum from the brighter quasar image B directly. During this first step, the PSF is constructed from the upper half of the spectrum in Fig. 18 containing the spectrum of image B. We then deconvolve the original data, we take the extended-channel part of the deconvolution, reconvolve it with the approximate PSF and subtract it from the data. This provides us with a spectrum of the quasar image that is much less affected by the lensing galaxy. A second PSF is constructed from these new lens-cleaned spectra and a new deconvolution is carried out. We perform this cycle twice to obtain the final spectrum presented in Fig. 19. This spectrum has a lower signal-to-noise than our MOS spectra and less accurate flux calibration but it allows to measure well the redshift of lens G2, which displays prominent [OII] emission, contrary to lens G1. Fig. 18 shows that the emission comes from an object lying outside the region delimited by the quasar image. It therefore clearly corresponds to lens G2.

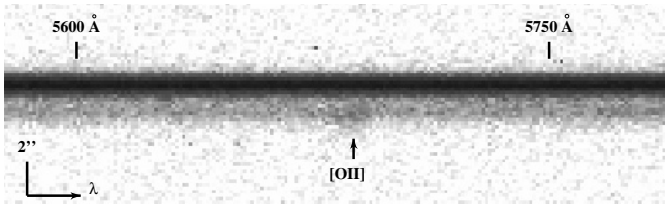

Fig. 18. Spectra of quasar image B and D of HE 0230−2130 (slit as in the middle panel of Fig. 17. A strong emission feature is seen "below" the quasar image D. It extends well beyond the area delimited by the quasar images, and corresponds to the [OII] emission of galaxy G2.

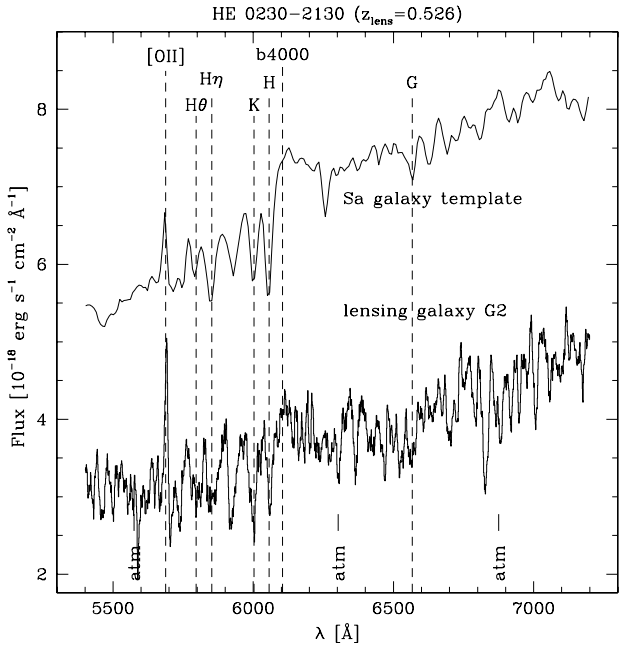

Fig. 19. Spectrum of the second lensing galaxy G2 in HE 0230−2130, obtained from the FORS1 long-slit spectrum. The exposure time is 3000 s. Note the prominent [OII] emission lines, absent from the spectrum of G1 (Fig. 10).

The redshift of lens G2 is $z_{\rm lens} = 0.526 \pm 0.002$. It is measured using the [OII] emission, the Ca II H & K absorption lines, the G-band, and the hydrogen Hθ and Hη absorption lines. The deconvolved spectrum of G2 is shown in Fig. 19. Although the flux calibration is not optimal without a good knowledge of the PSF, the spectrum resembles that of a Sa spiral galaxy.

As can be seen in the middle panel of Fig. 17, G2 is not well centered in the slit but lies at 0.4″ away from the slit center. This small *spatial* misalignment of the object within the slit mimics a spectral shift of ∼2 Å to the red. This translates into a redshift change of less than $\Delta z = 0.0004$ at 6000 Å and has no effect on the redshift determination of galaxy G2. We conclude that the observed difference in redshift $\Delta z = 0.003$ between galaxy G1 and G2 is real. It translates into a velocity difference of $\Delta v = 900 \pm 450$ km s^{-1} typical for a galaxy group. HE 0230−2130 might therefore be lensed by a group of physically related galaxies of which G1 and G2 are two of the main members.

5. Summary and conclusions

We present here the previously unknown redshifts of the lensing galaxies in three gravitationally lensed quasars and confirm four others, already presented in Ofek et al. (2005). We also measure the redshift of a second lensing galaxy in HE 0230−2130 and give a tentative estimate of the lens redshift in Q 1355−2257.

The MOS mode in which all observations are taken and the subsequent observation of several PSF stars is crucial to carry out a reliable decontamination of the lens spectrum by those of the quasar images. The PSF stars are also used to carry out a very accurate flux calibration of the spectra.

Contrary to long-slit observations where no PSF stars are available (Ofek et al. 2005), we do not need to iteratively remove a scaled version of the quasar spectra from the data. Because microlensing can produce significant differences between the spectra of the quasar images, such a procedure may result in biased continuum slopes and wrong conclusions about the presence of dust in the lens. For this reason we fully base our extraction on a spatial decomposition using independent PSF spectra.

We find that all the lensing galaxies in our sample are early-type ellipticals or S0, except for the second lensing galaxy in HE 0230−2130, which displays prominent [OII] emission. And we do not find any evidence for significant extinction by dust in their interstellar medium.

Acknowledgements. The authors are very grateful to the ESO staff at Paranal for the particular care paid to the slit alignment necessary to perform the spectra deconvolutions. P.M. acknowledge financial support from PRODEX (Belgium). COSMOGRAIL is financially supported by the Swiss National Science Foundation (SNSF). The image shown in Fig. 17 was obtained with the NASA/ESA Hubble Space Telescope (Program # 9744, PI: C. S. Kochanek) and extracted from the data archives at the Space Telescope Science Institute, which is operated by the Association of Universities for Research in Astronomy, Inc., under NASA contract NAS 5-26555.

References

Abajas, C., Mediavilla, E., Muñoz, J. A., Popović, L. Č., & Oscoz, A. 2002, ApJ, 576, 640
Agol, E., & Krolik, J. 1999, ApJ, 524, 49
Burles, S., et al. 2005, in preparation
Courbin, F., Magain, P., Kirkove, M., & Sohy, S. 2000, ApJ, 529, 1136
Eigenbrod, A., Courbin, F., Vuissoz, C., et al. 2005, A&A, 436, 25
Eigenbrod, A., Courbin, F., Dye, S., et al. 2006, 451, 747
Inada, N., et al. 2005, in preparation
Kinney, A. L., Calzetti, D., Bohlin, R. C., et al. 1996, ApJ, 467, 38
Magain, P., Courbin, F., & Sohy, S. 1998, ApJ, 494, 452
Mineshige, S., & Yonehara, A. 1999, PASJ, 51, 497
Morgan, N. D., Gregg, M. D., Wisotzki, L., et al. 2003, AJ, 126, 696
Morgan, N. D., Cardwell, J. A. R., Schechter, P. L., et al. 2004, AJ, 127, 2617
Morgan, N. D., Kochanek, C. S., Pevunova, O., & Schechter, P. L. 2005, AJ, 129, 2531
Ofek, E. O., Maoz, D., Rix, H.-W., Kochanek, C. S., & Falco, E. E. 2005 [arXiv:astro-ph/0510465]
Oguri, M., Inada, N., Castander, F. J., et al. 2004, PASJ, 56, 399
Refsdal, S. 1964, MNRAS, 128, 307
Saha, P., et al. 2005, A&A, submitted
Walsh, D., Carswell, R. F., & Weymann, R. J. 1979, Nature, 279, 381
Wisotzki, L., Christlieb, N., Liu, M. C., et al. 1999, A&A, 348, L41
Wisotzki, L., Schechter, P. L., Bradt, H. V., Heinmüller, J., & Reimers, D., et al. 2002, A&A, 395, 17
Wisotzki, L., Schechter, P. L., Chen, H.-W., et al. 2004, A&A, 419, L31